



Self-focusing of lemon and radial vector beam inside an atomic vapour

Partha Das, and Tarak Nath Dey

*Department of Physics, Indian Institute of Technology Guwahati,
Guwahati- 781 039, Assam, India*

We present gain-assisted focusing of vector beams (VBs) inside an atomic system. The atoms are prepared in a four-level configuration in an active Raman-gain scheme. The transitions are coupled by a σ polarized control field and two orthogonally polarized components of a probe VB. The probe beam can be self-focused inside the medium at two-photon resonance by choosing the suitable input beam intensities. We use the probability-amplitude method to calculate the linear and third-order nonlinear susceptibilities of both the components of the probe VB. We find the gain that is induced by the spatial intensity distribution of the strong control beam is mainly responsible for intending the probe beam to self-focus. Additionally, we investigate the polarization state of the VB at the minimum beam radius. The observed self-focusing of the VB results in a reduced spot size, which holds potential for applications in resolution enhancement. © Anita Publications. All rights reserved.

doi:[10.54955/AJP.33.11.2024.709-719](https://doi.org/10.54955/AJP.33.11.2024.709-719)

Keywords: Self-focusing, Vector beams, Kerr-nonlinearity.

1 Introduction

In recent years, there has been a growing interest in utilizing atomic coherence to manipulate the propagation of light within a medium. The self-focusing of light in a nonlinear medium has become a subject of significant interest in the field of nonlinear optics [1]. Self-focusing occurs when a light beam naturally concentrates due to the nonlinear refractive index induced by the medium. When a Gaussian beam with a bell-shaped symmetric transverse profile enters a nonlinear medium with refractive index $n = n_0 + \Delta n$ and $\Delta n(r) = n_2 I(r)$, the refractive index varies due to the transverse intensity profile of the beam. The central part of the beam travels through the medium with a higher refractive index, causing it to move more slowly than the edges. Consequently, as the beam propagates into the medium, the wavefront becomes increasingly distorted, resulting in self-focusing [2,3]. However, the diffracting action is inversely proportional to the square of the beam radius. Therefore, as the beam self-focuses and shrinks, both the self-focusing and diffracting action become stronger. If the former action grows faster than the latter, then diffraction eventually overcomes self-focusing, causing the beam to diffract. The concept of self-focusing was initially established in 1962 by Askaryan [4] and later supported by a theoretical model in 1964 [5,6]. Subsequently, Lallemand *et al* conducted experimental observations, while Vlasov *et al* provided an analytical explanation, introducing the method of moments to define the collapse distance [7-9]. The physical phenomenon of wave collapse has been observed in various contexts such as plasma waves [10], Bose-Einstein condensates or matter waves [11], capillary-gravity waves in deep water [12], and astrophysics [13]. Additionally, self-focusing and filamentation of the optical field have been observed in transparent media and in absorptive resonance gases [14,15]. Notably, during self-focusing, a high-power laser beam may undergo stimulated Raman scattering

Corresponding authors

e mail: tarak.dey@iitg.ac.in (Tarak N Dey)

(SRS), leading to the majority of its energy being transferred to a Stokes wave [16]. The phenomenon of gain-focusing for propagation in water is discussed in [17].

The production of Kerr nonlinearity and optical solitons has traditionally been achieved in passive optical media, such as glass-based optical fibers [18]. The nonlinear effect in passive optical media is considerably weak, necessitating either a long propagation distance or a high light intensity to accumulate sufficient nonlinear phase shifts and to form optical solitons. Electromagnetically induced transparency (EIT) has garnered attention in highly resonant optical media [19]. Through the quantum interference effect induced by a coupling laser field, EIT enables extensive suppression of the absorption of a probe laser field tuned to a strong one-photon resonance [20-22]. In contrast to the absorptive nature of the EIT-based scheme, active Raman gain (ARG) scheme have also garnered considerable theoretical and experimental interest [23-25]. The fundamental principle of the ARG scheme entails the amplification of the probe field through stimulated absorption by the control field. This system operates effectively at ambient temperature, minimizing both attenuation and distortion. Furthermore, it facilitates a notable enhancement of the Kerr nonlinearity of the probe field [26].

The effect of beam spreading can be mitigated by utilizing a self-focusing (Kerr) nonlinear medium. The disintegration of the orbital angular momentum (OAM) beams [27, 28] can be suppressed by employing VBs rather than scalar beams [29-31]. A VB or fully structured light (FSL) beam can be created through the vector superposition of two orthogonally polarized, OAM carrying Laguerre-Gaussian (LG) modes [32]. Cylindrical and Poincaré beams represent two categories of VB with net zero and nonzero OAM, respectively. The cylindrical VB features polarization profiles that are axially symmetric about the beam's propagation axis, including radial, azimuthal, and spiral polarization distributions [33], whereas the Poincaré beam exhibits radial and azimuthal variations of polarization in its lemon, star, and web polarization distributions [34,35]. Utilizing vector diffraction theory, the focusing characteristics and pattern alterations of axisymmetric Bessel-Gaussian, and Laguerre-Gaussian (LG) beams have been examined [36,37], presenting potential applications in the development of optical traps and chains of optical traps.

In this study, we have demonstrated the focusing of both cylindrical and Poincaré VB within an atomic vapor medium. The medium consists of a four-level ARG system, excited by a strong control field and the two orthogonal polarization components of the probe VB. Under two-photon resonance, the strong control field induces linear gain in the left-circularly polarized component of the probe VB through stimulated absorption, whereas the right-circularly polarized component experiences nonlinear absorption. The focusing of the VBs varies due to the medium's linear gain. Our work offers the advantage of discerning the polarization state of the focused beam within the medium, differentiating it from gain-focusing discussed in prior research on high-power laser beams propagating in water [17].

The paper is organized as follows. Section 1 offers a brief overview of self-focusing, its applications, and our research findings. The theoretical framework utilized in this investigation is outlined in Section 2. Section 3 details our research findings and provides comprehensive elucidations. Lastly, Section 4 contains the paper's concluding remarks.

2 Theoretical Formulation

2.1 Level System

In this paper, we present self-focusing of VBs while propagation through a medium. The system under consideration is a four-level ARG system where the probe field attains a linear gain along with nonlinear absorption due to the highly detuned control field coupled with the ground and the excited state. This configuration can be realized in ^{87}Rb $D_2(5^2S_{1/2} \rightarrow 5^2P_{3/2})$ transition hyperfine structure as: $|1\rangle = |5^2S_{1/2}, F=1, m_F=0\rangle$, $|2\rangle = |5^2S_{1/2}, F=2, m_F=0\rangle$, $|3\rangle = |5^2P_{3/2}, F=1, m_F=-1\rangle$, $|0\rangle = |5^2P_{3/2}, F=1, m_F=0\rangle$, and $|4\rangle = |5^2P_{3/2}, F=1, m_F=1\rangle$.

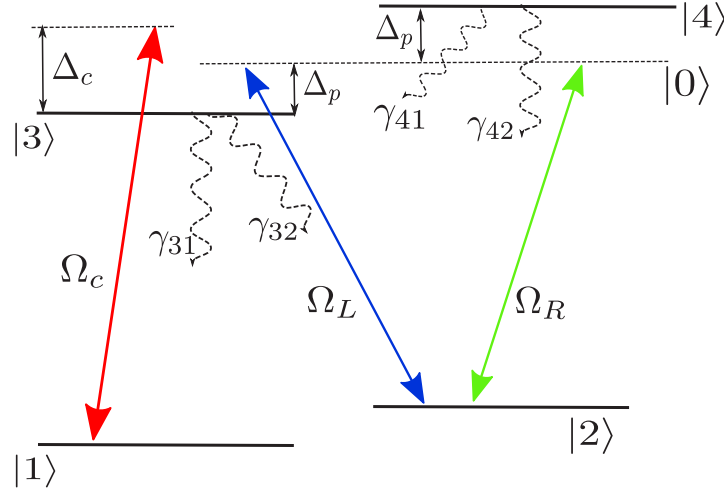


Fig 1. Schematic diagram of a four-level active-Raman-gain system. The right circularly polarized component, E_R , and the left circularly polarized component, E_L , of a weak probe VB drives the transitions $|2\rangle \leftrightarrow |4\rangle$ and $|2\rangle \leftrightarrow |3\rangle$, respectively. The transition $|1\rangle \leftrightarrow |3\rangle$ is coupled by a strong control field E_c . The spontaneous emission decay rate from $|3\rangle$ and $|4\rangle$ states are given by γ_{3j} and γ_{4j} ($j \in 1, 2$). The probe and control detunings are denoted by Δ_p , and Δ_c respectively.

The transitions $|1\rangle \leftrightarrow |3\rangle$ is coupled by a σ -polarized control field \vec{E}_c , which is defined as,

$$\vec{E}_c(r, t) = \hat{e}_\sigma \mathcal{E}_c(r) e^{-i(\omega_c t - k_c z)} + c.c., \quad (1)$$

where \hat{e}_σ , $\mathcal{E}_c(r)$, ω_c , k_c are the polarization vector, spatial envelop, central frequency and wavevector, respectively. A linear polarized vector probe field \vec{E}_p , can be resolved into two orthogonally polarized basis states $\hat{\sigma}_i$ ($i \in R, L$) as,

$$\vec{E}_p(r, t) = \hat{e}_x \mathcal{E}_p(r) e^{-i(\omega_p t - k_p z)} + c.c. \quad (2a)$$

$$= \sum_{i=R,L} \hat{\sigma}_i \mathcal{E}_i(r) e^{-i(\omega_p t - k_p z)} + c.c. \quad (2b)$$

where $\hat{\sigma}_{R(L)}$ represents the right (left) circular polarization unit vector, and the right (left)circular polarized component $\mathcal{E}_{R(L)}$ couples with the transition $|2\rangle \leftrightarrow |4\rangle$ ($|2\rangle \leftrightarrow |3\rangle$).

The time-dependent Hamiltonian that characterizes the interaction of the model system, can be expressed under dipole approximation as,

$$\mathbf{H} = \mathbf{H}_0 + \mathbf{H}_I, \quad (3a)$$

$$\mathbf{H}_0 = \hbar(\omega_{21}|2\rangle\langle 2| + \omega_{31}|3\rangle\langle 3| + \omega_{41}|4\rangle\langle 4|), \quad (3b)$$

$$\begin{aligned} \mathbf{H}_I &= -\hat{d} \cdot \vec{E} \\ &= -[\vec{d}_{42} \cdot (\hat{e}_R \mathcal{E}_R e^{-i\omega_p t} + c.c.)|4\rangle\langle 2| + \vec{d}_{32} \cdot (\hat{e}_L \mathcal{E}_L e^{-i\omega_p t} + c.c.)|3\rangle\langle 2| \\ &\quad + \vec{d}_{31} \cdot (\hat{e}_\sigma \mathcal{E}_c e^{-i\omega_c t} + c.c.)|3\rangle\langle 1|] + \text{H.c.}, \end{aligned} \quad (3c)$$

where ω_{j1} ($j = 2, 3, 4$) correspond to the frequency separation between the state $|j\rangle$ and the ground state $|1\rangle$ and \vec{d}_{3k} ($k = 1, 2$), \vec{d}_{42} are the matrix elements of the induced dipole moments for the transitions $|3\rangle \leftrightarrow |k\rangle$, and $|4\rangle \leftrightarrow |2\rangle$, respectively. To eliminate the explicit time dependence in the Hamiltonian, we use the following unitary transformation

$$U = \exp[-i\omega_c t (|3\rangle\langle 3| + |4\rangle\langle 4|) - i(\omega_c - \omega_p) t |2\rangle\langle 2|]. \quad (4)$$

The effective Hamiltonian in the interaction picture can be expressed as, $\mathcal{H} = \hat{U}^\dagger H \hat{U} - i\hbar \hat{U}^\dagger \partial_t \hat{U}$. When applying the rotating wave approximation (RWA), this yields

$$\begin{aligned} \mathcal{H} = & -\hbar[(\Delta_c - \Delta_p)|2\rangle\langle 2| + \Delta_c|3\rangle\langle 3| + (\Delta_c - 2\Delta_p)|4\rangle\langle 4|] \\ & -\hbar[\Omega_c|3\rangle\langle 1| + \Omega_L|3\rangle\langle 2| + \Omega_R|4\rangle\langle 2|] + \text{H.c.} \end{aligned} \quad (5)$$

The single photon detunings of the probe and control field for their respective transitions are denoted as:

$$\Delta_c = \omega_c - \omega_{31}, \Delta_p = \omega_p - \omega_{02}, \quad (6)$$

and the Rabi frequencies of probe field components and control field is expressed as:

$$\Omega_c = \frac{\vec{d}_{31} \cdot \hat{e}_\sigma}{\hbar} \mathcal{E}_c, \Omega_L = \frac{\vec{d}_{32} \cdot \hat{e}_L}{\hbar} \mathcal{E}_L, \Omega_R = \frac{\vec{d}_{42} \cdot \hat{e}_R}{\hbar} \mathcal{E}_R. \quad (7)$$

Using the probability-amplitude method we get the equations of motion for the atomic response which are given as:

$$i\dot{C}_1 + \Omega_c^* C_3 = 0, \quad (8a)$$

$$i\dot{C}_2 + d_2 C_2 + \Omega_L^* C_3 + \Omega_R^* C_4 = 0, \quad (8b)$$

$$i\dot{C}_3 + d_3 C_3 + \Omega_c C_1 + \Omega_L C_2 = 0, \quad (8c)$$

$$i\dot{C}_4 + d_4 C_4 + \Omega_R C_2 = 0, \quad (8d)$$

where, $\sum_{i=1}^4 |C_i|^2 = 1$, C_i ($i \in 1, 2, 3, 4$) is the probability amplitude of the bare state. In Eq (8), $d_2 = (\Delta_c - \Delta_p + i\gamma_2)$, $d_3 = (\Delta_c + i\gamma_3)$, $d_4 = (\Delta_c - 2\Delta_p + i\gamma_4)$ with γ_j ($j \in 2, 3, 4$) being the atomic decay rates from the states $|j\rangle$.

2.1 Stokes Parameters

The description of any light's polarization state necessitates the use of the four Stokes polarization parameters. To comprehend the state of polarization in the transverse plane of the VB, it can be decomposed into its two orthogonally polarized LG modes. A circular polarization basis of the VB can be derived in the following manner:

$$\vec{E}(r, \phi, z) = \mathcal{E}_L(r, \phi, z)\hat{e}_L + \mathcal{E}_R(r, \phi, z)\hat{e}_R, \quad (9)$$

where,

$$\mathcal{E}_L(r, \phi, z) = \cos(\alpha) LG_0^{i_L}, \mathcal{E}_R(r, \phi, z) = \sin(\alpha)e^{i\theta} LG_0^{i_R} \quad (10)$$

\mathcal{E}_L , and \mathcal{E}_R are the two orthogonal polarized component of the VB. The relative amplitude and phase of the two modes is defined by α , and θ , respectively. The spatial modes, $LG_0^{i_i}$ ($i = L, R$), refer to the Laguerre Gaussian polynomial, having radial index zero and is given by

$$LG_0^{i_i}(r, \phi, z) = \mathcal{E}_0 \sqrt{\frac{2}{\pi|l_i|!}} \left(\frac{r\sqrt{2}}{w(z)} \right)^{|l_i|} e^{-\frac{r^2}{w(z)^2}} e^{il_i\phi + ik_i n_i z} \exp\left(\frac{ik_i n_i r^2 z}{2(z^2 + n_i^2 z_R^2)} \right) e^{-(|l_i| + 1)\eta(z)} \quad (11)$$

$w(z) = w_0 \sqrt{1 + z^2/n_i^2 z_R^2}$ defines the beam radius at a propagation length z , where w_0 represents the beam waist at $z = 0$, and n_i is the refractive index. The parameter $z_R = k_i w^2/2$ denotes the free space Rayleigh length, with k_i being the free space wave number. The OAM index is l_i , and the Gouy phase can be expressed as $(|l_i| + 1)\eta(z)$, where $\eta(z) = \tan^{-1}(z/n_i z_R)$. The refractive indices, $n_R = 1 + 2\pi\text{Re}[\chi_{42}]$, and $n_L = 1 + 2\pi\text{Re}[\chi_{32}]$. The Stokes parameters in the circular basis are expressed as:

$$S_0 = |\mathcal{E}_R|^2 + |\mathcal{E}_L|^2, S_1 = 2\text{Re}[\mathcal{E}_R^* \mathcal{E}_L], S_2 = 2\text{Im}[\mathcal{E}_R^* \mathcal{E}_L], S_3 = |\mathcal{E}_L|^2 - |\mathcal{E}_R|^2. \quad (12)$$

From Eq (12), we can calculate the ellipticity, ζ and the orientation, ξ of polarization at each point in the transverse plane as:

$$\frac{S_1}{S_0} = \cos(2\zeta) \cos(2\xi), \quad \frac{S_2}{S_0} = \cos(2\zeta) \sin(2\xi), \quad \frac{S_3}{S_0} = \sin(2\zeta), \quad (13)$$

which give

$$\zeta = \frac{1}{2} \sin^{-1} \left(\frac{S_3}{S_0} \right), \quad \xi = \frac{1}{2} \tan^{-1} \left(\frac{S_2}{S_1} \right). \quad (14)$$

We substitute Eqs (10), (11), and (12) in Eq (14) assuming that the free space wave vector $k_R = k_L = k$, gives

$$\zeta(z) = -\frac{1}{2} \left[\theta + \phi \Delta(l_{L,R}) + kz \Delta(n_{R,L}) + \eta(z) \Delta(|l_{L,R}|) + \frac{kzr^2}{2} \left\{ \frac{n_R}{z^2 + n_R^2 z_R^2} - \frac{n_L}{z^2 + n_L^2 z_R^2} \right\} \right], \quad (15)$$

where $\Delta(l_{L,R}) = l_L - l_R$, $\Delta(|l_{L,R}|) = |l_L| - |l_R|$, and $\Delta(n_{R,L}) = n_R - n_L$. Subsequently, following propagation through a distance z within the medium, the polarization of aVB at each point on the transverse plane undergoes a rotation determined by the following expression:

$$\Delta \zeta(z) = -\frac{\Delta |l_{L,R}| \eta(z)}{2} - \frac{1}{2} \left[\frac{kzr^2}{2} \left\{ \frac{n_R}{z^2 + n_R^2 z_R^2} - \frac{n_L}{z^2 + n_L^2 z_R^2} \right\} + kz \Delta(n_{R,L}) \right], \quad (16)$$

According to the Eq (16), it is apparent that the polarization the medium in the case of CV beams arises exclusively from the disparity in the refractive index of the two constituents of the probe beam. In addition, the change in ellipticity of the VB beam can also be represented as:

$$\Delta \zeta(z) = \frac{1}{2} \left[\sin^{-1} \left\{ \frac{1 - a \tan^2 \alpha}{1 + a \tan^2 \alpha} \right\} - \sin^{-1} \left\{ \frac{1 - b \tan^2 \alpha}{1 + b \tan^2 \alpha} \right\} \right], \quad (17)$$

where,

$$a = \exp \left[\frac{2r^2}{w_0^2} \left(\frac{n_R^2 z_R^2}{z^2 + n_R^2 z_R^2} - \frac{n_L^2 z_R^2}{z^2 + n_L^2 z_R^2} \right) \right] \left(\frac{r\sqrt{2}}{w_0 \sqrt{1 + z^2/n_R^2 z_R^2}} \right)^{2|l_R|} \left(\frac{r\sqrt{2}}{w_0 \sqrt{1 + z^2/n_L^2 z_R^2}} \right)^{-2|l_L|} \quad (18)$$

and

$$b = \left(\frac{r\sqrt{2}}{w_0} \right)^{2(|l_R| - |l_L|)}. \quad (19)$$

2.3 Linear and nonlinear (Kerr) susceptibilities

In this section, our objective is to compute both linear and third order nonlinear susceptibilities of the medium. The nonlinear Kerr susceptibility holds great importance in the field of nonlinear optics, where it plays a crucial role in various optical phenomena. It specifically pertains to the third-order nonlinear optical susceptibility ($\chi^{(3)}$) that gives rise to the Kerr effect. This effect manifests as an intensity-dependent alteration in the refractive index of a material, and is characterized by the real part of third-order optical susceptibilities. The probe-field susceptibility is precisely defined as

$$\chi_{32} \equiv \chi_L = \frac{\mathcal{N} |d_{23}|^2}{\hbar} \left(\frac{C_3 C_2^*}{\Omega_L} \right) \simeq \chi_L^{(1)} + \chi_{LL}^{(3)} |\Omega_L|^2 + \chi_{LR}^{(3)} |\Omega_R|^2, \quad (20a)$$

$$\chi_{42} \equiv \chi_R = \frac{\mathcal{N} |d_{24}|^2}{\hbar} \left(\frac{C_4 C_2^*}{\Omega_R} \right) \simeq \chi_R^{(1)} + \chi_{RR}^{(3)} |\Omega_R|^2 + \chi_{RL}^{(3)} |\Omega_L|^2, \quad (20b)$$

where, \mathcal{N} is the atomic density of the medium. The linear probe susceptibility is denoted as $\chi_{LR}^{(1)}$, while the third order self and cross Kerr susceptibilities are represented as $\chi_{LL,RR}^{(3)}$ and $\chi_{LR,RL}^{(3)}$, respectively. We solve Eq (8) under steady-state conditions. The probability amplitudes are obtained by satisfying the condition $\sum_{i=1}^4 |C_i|^2 = 1$. Hence

$$C_1 = \left[1 + |\Omega_c|^2 \frac{|D_s|^2 + |\Omega_L|^2 (|\Omega_R|^2 + |d_4|^2)}{|D|^2} \right]^{1/2} \quad (21)$$

where, $D_s = |\Omega_R|^2 - d_2 d_4$, and $D = d_4 |\Omega_L|^2 + d_3 |\Omega_R|^2 - d_2 d_3 d_4$. The other probability amplitudes can be written in terms of C_1 as:

$$C_2 = -\frac{d_4 \Omega_L^* \Omega_c}{D} C_1, \quad (22a)$$

$$C_3 = -\frac{D_s \Omega_c}{D} C_1, \quad (22b)$$

$$C_4 = \frac{\Omega_L^* \Omega_c \Omega_R}{D} C_1. \quad (22c)$$

In order to derive the linear and nonlinear susceptibilities as defined in Eq (20), a Taylor expansion is performed around $|\Omega_L|^2 = |\Omega_R|^2 = 0$, resulting in the following expressions:

$$\chi_L^{(1)} = -\frac{\mathcal{N} |d_{23}|^2}{\hbar} \frac{|\Omega_c|^2}{d_2^* (|d_3|^2 + |\Omega_c|^2)}, \quad (23a)$$

$$\chi_{LL}^{(3)} = -\frac{\mathcal{N} |d_{23}|^2}{\hbar} \frac{|\Omega_c|^2 d_2^* d_3^* + d_2 d_3 - |\Omega_c|^2}{d_2^* |d_2|^2 (|d_3|^2 + |\Omega_c|^2)^2}, \quad (23b)$$

$$\chi_{LR}^{(3)} = -\frac{\mathcal{N} |d_{23}|^2}{\hbar} \frac{|\Omega_c|^2 d_2 d_4}{d_2^* |d_2|^2 (|d_3|^2 + |\Omega_c|^2)}, \quad (23c)$$

$$\chi_R^{(1)} = \chi_{RR}^{(3)} = 0, \quad (23d)$$

$$\chi_{RL}^{(3)} = -\frac{\mathcal{N} |d_{24}|^2}{\hbar} \frac{|\Omega_c|^2}{|d_2|^2 d_4 (|d_3|^2 + |\Omega_c|^2)}. \quad (23e)$$

In the preceding equations, it can be observed that the right component of the probe VB, connected to the transition $|2\rangle \leftrightarrow |4\rangle$, exhibits only cross Kerr susceptibility.

2.4 Propagation equation

The investigation of beam propagation equations plays a pivotal role in examining the influence of absorption, diffraction, dispersion, and anisotropy on VB propagation. By employing the slowly varying envelope and paraxial wave approximations, the propagation equations governing the right and left circularly polarized components of the probe VB can be written as:

$$\frac{\partial \Omega_R}{\partial z} = \frac{i}{2k_R} \nabla_{\perp}^2 \Omega_R + 2\pi i k_R \chi_R \Omega_R \quad (24a)$$

$$\frac{\partial \Omega_L}{\partial z} = \frac{i}{2k_L} \nabla_{\perp}^2 \Omega_L + 2\pi i k_L \chi_L \Omega_L \quad (24b)$$

The right-hand side of the equation consists of two terms: the first term accounts for diffraction, while the second term denotes the dispersion and absorption of the probe VB. It is important to note that the propagation equations are interconnected through the susceptibilities χ_R and χ_L . The dynamics of the strong control field E_c is disregarded due to the specific geometrical structure and polarization characteristics. To numerically analyze Eqs (24a) and (24b), the split-step Fourier method (SSFM) has been selected for the study.

3 Results and discussion

3.1 Linear and nonlinear (Kerr) susceptibilities of probe VB

In this section, we present the response of linear and nonlinear susceptibilities for the two components of the probe VB. In Figs 2 (a)-(b), the response corresponds to the left circularly polarized component, while Figs 2 (c)-(d) denote the right circularly polarized component of the probe beam. In Fig 2(a), it is observed that $\text{Re}[\chi^{(1)}]$ and $\text{Re}[\chi^{(3)}]$ are zero at the two-photon resonance, while $\text{Re}[\chi^{(3)}]$ is nonzero. Additionally, Fig 2(b) indicates that linear gain is accompanied by nonlinear absorption. Interestingly, Figs 2 (c)-(d) reveal that the right circularly polarized component exclusively exhibits cross-Kerr susceptibilities, as expected by the model system, where the coherence $C_4C_2^*$ is nonzero in the presence of the left circular component. Notably, our work is conducted in the paraxial regime throughout the paper, which is valid as our beam waist is much larger than the wavelength.

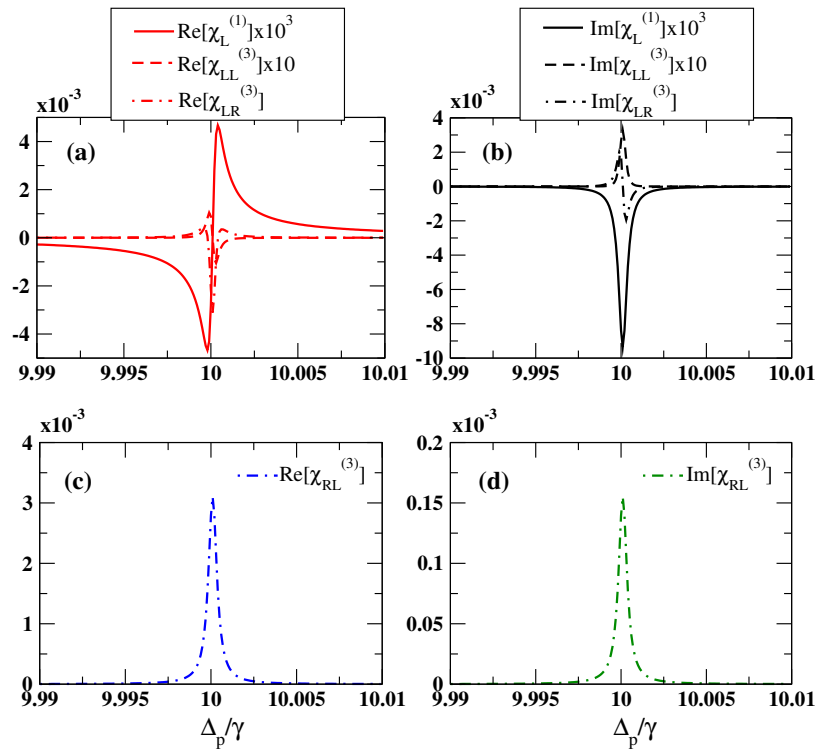


Fig 2. Real and imaginary parts of both linear and third-order nonlinear χ_L and χ_R are plotted against the corresponding transition detunings. (a), (b) correspond to real, and imaginary part of χ_L plotted against $\Delta p/\gamma$, respectively. Similarly (c), (d) correspond to real, and imaginary part of χ_R plotted against $\Delta p/\gamma$, respectively. Parameters used: $\Omega_{R,L} = 0.001\gamma$, $\Omega_c = 0.7\gamma$, $\gamma_2 = 3 \times 10^{-4}\gamma$, $\gamma_3 = 5 \times 10^2\gamma$, $\gamma_4 = 0.5\gamma$, $\Delta_c = 10\gamma$. The density of atoms, $N = 5 \times 10^{11}\text{cm}^{-3}$.

3.2. Focusing of lemon and radial VB

In order to achieve self-focusing of the probe VB, the transverse spatial profile of the control beam must be selected so that its central intensity exceeds that of the tail. To accomplish this, we have opted for a Gaussian beam and a super-Gaussian control beam for the propagation of the lemon and radial VB, respectively. The control field is defined as,

$$\Omega_c(r, \phi, 0) = \Omega_{c0} \exp \left[- \left(\frac{r^2}{w_0^2} \right)^{l_c} \right]. \quad (25)$$

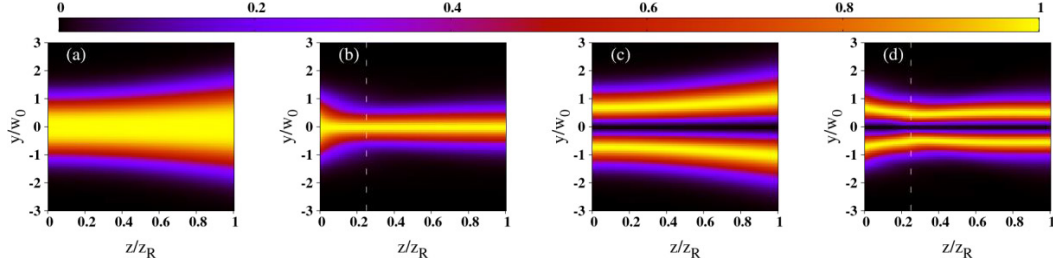


Fig 3. Longitudinal intensity profile of (a) lemon ($l_L = 0$, $l_R = 1$, $\alpha = \pi/4$, $\theta = 0$), (b) radial ($l_L = -1$, $l_R = 1$, $\alpha = \pi/8$, $\theta = 0$) VB propagating in free space, and inside the gain medium (c), and (d), respectively. The value of l_c for the propagation of lemon and radial VB is taken as 1, and 4, respectively. The probe and the control beam have a waist, $w_0 = 50\mu\text{m}$ and is maintained consistently. White dashed vertical line denotes the minimum spot size achieved due to self-focusing. Other parameters are same as Fig 2.

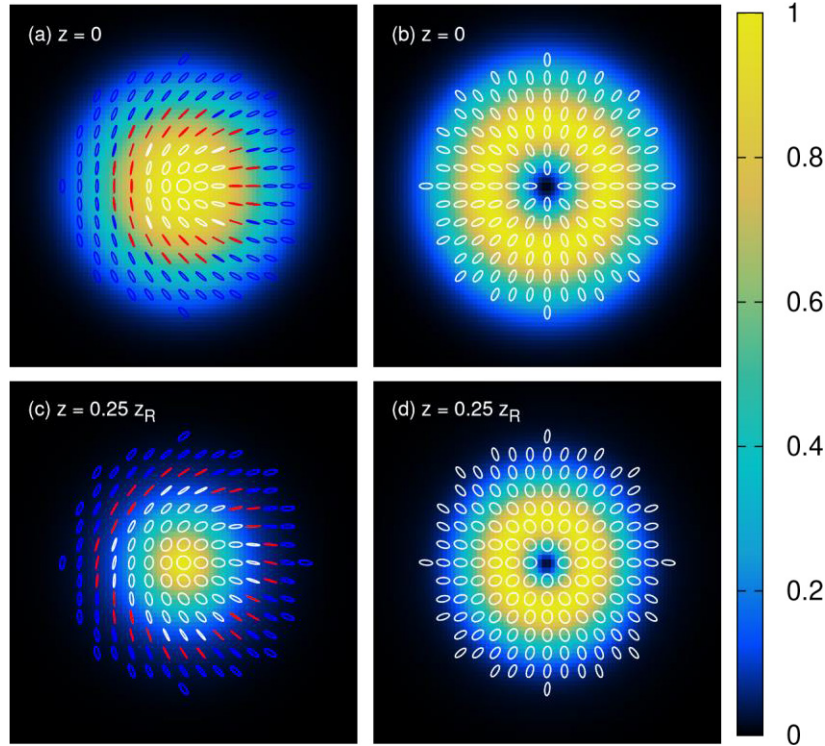


Fig 4. Transverse intensity and polarization distribution at the $z = 0$ for (a) lemon, (b) radial and at minimum beam radius $z = 0.25z_R$ for (c) lemon, (d) radial VB, respectively. The intensity is normalized by its maximum intensity for each VB. The colors white, red, and blue correspond to left circular, linear, and right circular polarizations, respectively. Parameters remain same as Fig 2.

The input amplitude of the control beam is denoted by Ω_{c0} . In the figures labeled as 3 (a)-(d), we illustrate the propagation of VBs in both free space and within the Raman gain medium. During the initial self-focusing phase, the control beam facilitates energy transfer to the probe beam. The energy transfer is more pronounced in regions with higher control beam intensity, resulting in a gain-narrowed probe profile

that achieves a minimum spot radius. In the illustrations labeled Fig 3 (a) and Fig 3 (c), the longitudinal profile of lemon and radial VB propagation in free space is depicted. Conversely, Fig 3(b) and Fig 3(d) characterize the propagation of lemon and radial VB inside the medium. The left circularly polarized component of the probe VB experiences linear gain, thereby facilitating beam self-focusing. As self-focusing reduces the beam diameter, diffraction increases, and beyond a certain distance, the beam undergoes diffraction, a phenomenon known as gain-focusing. Refractive focusing is attributed to the real part, while gain focusing is linked to the imaginary part of the susceptibility of the probe beam. The discussed gain-focusing phenomenon is expected to be a pervasive occurrence, applicable to any medium supporting nonlinear focusing and stimulated Raman scattering.

Further, we examine the state of polarization (SOP) of the probe VBs both at the input and after focusing to the minimum beam radius. As depicted in Fig 4(a) and Fig 4(b), we display the SOP at input $z = 0$ for the lemon and radial VBs, respectively. Subsequently, after the beam focuses, the SOP of the lemon and radial VBs at $z = 0.25z_R$ is illustrated by Fig 4(c) and Fig 4(d) correspondingly. Our findings indicate that the SOP of the lemon VB at $z = 0.25z_R$ has undergone a clockwise rotation by an angle of $\pi/4$ with a variation in ellipticity. Conversely, in the case of the radial VB, the SOP remains relatively unchanged, attributable to the insubstantial difference between $\text{Re}[\chi_{32}]$ and $\text{Re}[\chi_{42}]$. Moreover, we observe that the full width at half maximum (FWHM) of the lemon VB at the input is $1.84w_0$, which subsequently becomes $0.84w_0$ upon focusing at $z = 0.25z_R$. Likewise, at the input, the FWHM of the central dark region of the radial VB is $0.68w_0$, reduced to $0.44w_0$ upon focusing. Hence, it is imperative to carefully consider the intensity of the probe and control beam to achieve moderate gain, leading to the focusing of the VBs.

4 Conclusion

To summarize, we have utilized a theoretical model to control the susceptibility of the medium in order to achieve beam focusing of lemon and radial VBs within atomic vapor. Furthermore, we have examined the state of polarization of the VBs at both the initial and the minimum beam radius. The system under consideration consists of a control field with a Gaussian or super-Gaussian transverse intensity profile and two perpendicular components of probe VBs. At two-photon resonance, the combination of linear gain and nonlinear absorption leads to beam focusing. The transverse variation of the control beam profile is replicated in the linear gain profile. This phenomenon, known as gain focusing, occurs as the imaginary part of the susceptibility, which provides linear gain, is primarily responsible for beam focusing. The implementation of self-focusing has led to a reduction in the spot size of the beam, potentially offering benefits in improving resolution.

Acknowledgment

We gratefully acknowledges funding by the Department of Science and Technology, Anusandhan National Research Foundation, Government of India (Grant No. CRG/2023/001318).

References

1. Boyd R W, Lukishova S G, Shen Y R (eds), *Self-focusing: Past and present: Fundamentals and prospects*, (Springer Science), 2009.
2. Shen Y R, *Self-focusing: Experimental*, *Prog Quantum Electron*, 4(1975)1–34.
3. Marburger J H, *Self-focusing: Theory*, *Prog. Quantum Electron*, 4(1975)35–110.
4. Askaryan G A, *Cerenkov radiation and transition radiation from electromagnetic waves*, *J Exptl Theoret Phys*, 42(1962)1360–1364.
5. Chiao R Y, Garmire E, Townes C H, *Self-trapping of optical beams*, *Phys Rev Lett*, 13(1964)479–482.
6. Kelley P L, *Self-focusing of optical beams*, *Phys Rev Lett*, 15(1965)1005–1008.

7. Lallemand P, Bloembergen N, Self-focusing of laser beams and stimulated raman gain in liquids, *Phys Rev Lett*, 15(1965)1010–1012.
8. Garmire E, Chiao R Y, Townes C H, Dynamics and characteristics of the self-trapping of intense light beams, *Phys Rev Lett*, 16(1966)347–349.
9. Vlasov S N, Petrishchev V A, Talanov V I, Averaged description of wave beams in linear and nonlinear media (the method of moments), *Radiophys Quantum Electron*, 14(1971)1062–1070.
10. Wong A Y, Cheung P Y, Three-dimensional self-collapse of langmuir waves, *Phys Rev Lett*, 52(1984)1222–1225.
11. Sackett C A, Gerton J M, Welling M, Hulet R G, Measurements of collective collapse in a bose-einstein condensate with attractive interactions, *Phys Rev Lett*, 82(1999)876–879.
12. Banerjee P P, Korpel A, Lonngren K E, Self-refraction of nonlinear capillary-gravity waves, *Phys Fluids*, 26(1983)2393–2398.
13. Houbiers M, Stoof H T C, Stability of bose condensed atomic ^7Li , *Phys Rev A*, 54(1996)5055–5066.
14. Grischkowsky D, Self-focusing of light by potassium vapor, *Phys Rev Lett*, 24(1970)866–869.
15. Wang Y, Nonlinear self-focusing in cold Cesium atoms, (The University of Wisconsin-Madison), 2005.
16. Helle M H, Jones T G, Pen˜ano J R, Kaganovich D, Ting A, Formation and propagation of meter-scale laser filaments in water, *Appl Phys Lett*, 103(2013)121101; doi.org/10.1063/1.4821447.
17. Hafizi B, Palastro J P, Pen˜ano J R, Gordon D F, Jones T G, Helle M H, Kaganovich D, Stimulated raman scattering and nonlinear focusing of high-power laser beams propagating in water, *Opt Lett*, 40(2015)1556–1558.
18. Soman S K O, A tutorial on fiber kerr nonlinearity effect and its compensation in optical communication systems, *J Opt*, 23(2021)123502; doi. 10.1088/2040-8986/ac362a.
19. Fleischhauer M, Imamoglu A, Marangos J P, Electromagnetically induced transparency: Optics in coherent media, *Rev Mod Phys*, 77(2005)633–673.
20. Wu Y, Deng L, Ultraslow optical solitons in a cold four-state medium, *Phys Rev Lett*, 93(2004)143904; doi.org/10.1103/PhysRevLett.93.143904.
21. Huang G, Jiang K, Payne M G, Deng L, Formation and propagation of coupled ultraslow optical soliton pairs in a cold three-state double- Λ system, *Phys Rev E*, 73(2006)056606; doi.org/10.1103/PhysRevE.73.056606.
22. Hang C, Huang G, Deng L, Generalized nonlinear schrödinger equation and ultraslow optical solitons in a cold four-state atomic system, *Phys Rev E*, 73(2006)036607; doi.org/10.1103/PhysRevE.73.036607.
23. Stenner M D, Gauthier D J, Pump-beam-instability limits to raman-gain-doublet “fast-light” pulse propagation, *Phys Rev A*, 67(2003)063801; doi.org/10.1103/PhysRevA.67.063801.
24. Jiang K J, Deng L, Payne M G, Superluminal propagation of an optical pulse in a doppler-broadened three-state single-channel active raman gain medium, *Phys Rev A*, 76(2007)033819; doi.org/10.1103/PhysRevA.76.033819.
25. Deng L, Payne M G, Gain-assisted large and rapidly responding kerr effect using a room-temperature active raman gain medium, *Phys Rev Lett*, 98(2007)253902; doi.org/10.1103/PhysRevLett.98.253902.
26. Hang C, Huang G, Giant kerr nonlinearity and weak-light superluminal optical solitons in a four-state atomic system with gain doublet, *Opt Express*, 18(2010)2952–2966.
27. Firth W J, Skryabin D V, Optical solitons carrying orbital angular momentum, *Phys Rev Lett*, 79(1997)2450–2453.
28. Desyatnikov A S, Kivshar Y S, Necklace-ring vector solitons, *Phys Rev Lett*, 87(2001)033901; doi.org/10.1103/PhysRevLett.87.033901.
29. Zhu Z H, Chen P, Li H W, Zhao B, Zhou Z Y, Hu W, Gao W, Lu Y Q, Shi B S, Fragmentation of twisted light in photon-phonon nonlinear propagation, *Appl Phys Lett*, 112(2018)161103; doi.org/10.1063/1.5020082.
30. Bigelow M S, Zerom P, Boyd R W, Breakup of ring beams carrying orbital angular momentum in sodium vapor, *Phys Rev Lett*, 92(2004)083902.
31. Izdebskaya Y V, Rebling J, Desyatnikov A S, Kivshar Y S, Observation of vector solitons with hidden vorticity, *Opt Lett*, 37(2012)767–769.
32. Yao A M, Padgett M J, Orbital angular momentum: origins, behavior and applications, *Adv Opt Photon*, 3(2011)161–204.
33. Zhan Q, Cylindrical vector beams: from mathematical concepts to applications, *Adv Opt Photon*, 1(2009)1–57.

34. Galvez E J, Khadka S, Schubert W H, and Nomoto S, Poincaré-beam patterns produced by nonseparable superpositions of laguerre–gauss and polarization modes of light, *Appl Opt*, 51(2012)2925–2934.
35. Beckley A M, Brown T G, Alonso M A, Full poincaré beams, *Opt Express*, 18(2010)10777–10785.
36. Qiufang Z, Rongfu Z, Sitong D, Guanxue W, and Xiumin G, Focusing pattern of axisymmetric bessel–gaussian beam with helical polarization under triangular modulation, *Appl Opt*, 59(2020)648–652.
37. Lu C, Li J, Zhang H, Li S, Gao X, Focusing pattern of the laguerre–gaussian beam with polarization mixing helical-conical phase modulation, *J Opt Soc Am A*, 40(2023)1303–1309.

[Received: 01.10.2024; rev recd: 28.11.2024; accepted: 30.11.2024]